Effect of Wall Cooling on the Stability of Compressible Subsonic Flows Over Smooth Humps and Backward-Facing Steps

by

Ayman A. Al-Maaitah, Ali H. Nayfeh, and Saad A. Ragab

Department of Engineering Science and Mechanics

Virginia Polytechnic Institute and State University

Blacksburg, Virginia 24061

Abstract

The effect of wall cooling on the two-dimensional linear stability of subsonic flows over two-dimensional surface imperfections is investigated. Results are presented for flows over smooth humps and backward-facing steps with Mach numbers up to 0.8. The results show that, whereas cooling decreases the viscous instability, it increases the shear-layer instability and hence it increases the growth rates in the separation region. The coexistence of more than one instability mechanism makes a certain degree of wall cooling most effective. For the Mach numbers 0.5 and 0.8, the optimum wall temperatures are about 80% and 60% of the adiabatic wall temperature, respectively. Increasing the Mach number decreases the effectiveness of cooling slightly and reduces the optimum wall temperature.

I. Introduction

Due to proven achievability of Natural Laminar Flow[1] (NLF), there is an increasing interest to use it for the design of high performance aircraft. The substantial drag reduction with NLF has promoted more analyses of ways to achieve and maintain NLF on airfoils and other aerodynamic geometries. The maintenance of NLF is critically sensitive to the location of transition, which is strongly affected by surface imperfections. Since many of these imperfections cannot be avoided by modern

manufacturing techniques[2,3], a guide is needed for their allowable sizes and methods that should be used to control their effect on NLF.

There are some empirically based criteria in the literature[4,5] for prediction of the transition of flows around imperfections. But these criteria are for special cases and geometries, and they do not explain the instability mechanisms enhanced by the imperfections or the physics of ways to control them. Nayfeh, Ragab, and Al-Maaitah[6] studied analytically the stability of incompressible flows around two-dimensional (2-D) bulges; their method accounted for both viscous and shear-layer instabilities. They also correlated their results with the experiments of Walker and Greening[7] and found that the e^N method can be used to predict transition around 2-D bulges. Bestek et al[8] solved the unsteady Navier-Stokes equations using finite-differences; they concluded that the unsteadiness of the separated flow can be regarded as a phenomenon governed by the hydrodynamic instability. Their calculations show that Tollmien-Schlichting waves amplify considerably once the separation is enhanced in agreement with the results of Nayfeh et al[6]. Burnel et al[9] and Gougat and Martin[10] experimentally investigated the flow over 2-D imperfections. Their measurements of the amplified disturbances show that they damp down in the region of favorable pressure gradient. A similar trend is seen in the calculations of Nayfeh et al[6].

Recently, the effect of compressibility on the achievability of NLF has received more attention for non-lifting surfaces. High subsonic and supersonic Mach-number flows develop density gradients across the boundary layer, which provide additional damping to 2-D and axisymmetric T-S waves. For certain geometricies this advantage can be offset by the increase in the adverse pressure gradients. Vijgen et al[11] showed that increasing the freestream Mach number has a stabilizing effect on subsonic laminar boundary layers over fuselages. Their Mach number varied from low subsonic to 0.8. Hastings et al[12] reported that NLF extended as far as 37% on a NLF fairing installed on a turbo fan nozzle.

In spite of the previous investigations more understanding of the physics of the instability of such flows and ways to control them are still needed, especially for compressible flows. The two most common ways for laminar flow control are wall cooling in air (or heating in water) and wall suction. Wall cooling stabilizes incompressible flows over flat plates in air and destabilizes them in water[13-16]. Mack[17] and Malik[18] found that for compressible flows, wall cooling stabilizes the first mode but destabilizes the second mode. The question to be asked is how does wall

cooling affect flows around surface imperfections, and whether these flows can be stabilized by this technique, especially, since there is an interaction of more than one instability mechanism.

The purpose of this work is to study the effect of wall cooling on the subsonic two-dimensional stability of boundary layers around two-dimensional smooth backward-facing steps and humps.

II. Mean Flow

The sizes of the two-dimensional imperfections under consideration are such that strong viscous-inviscid interactions and small separation bubbles are unavoidable. The conventional laminar boundary-layer formulation cannot predict such flows. An alternative is to solve the full Navier-Stokes equations, but in such a case the grid should be so fine that important flow characteristics are not smeared by the truncation error and artificial dissipation. However, due to the large number of cases need to be investigated, solving the full Navier-Stokes equations is a very expensive task. A more economical alternative is to solve the interacting boundary-layer (IBL) equations or the nonlinear triple-deck equations.

We calculated the two-dimensional compressible laminar boundary layers over flat plates with 2-D surface imperfections using the interacting boundary-layer equations (IBL). The flowfield is assumed to be governed by the steady compressible boundary-layer equations as follows:

x-momentum equation

$$\rho u \frac{\partial u}{\partial x} + \rho v \frac{\partial u}{\partial y} = -\frac{dp}{dx} + \frac{1}{Re}\frac{\partial}{\partial y}\left(\mu \frac{\partial u}{\partial y}\right) \tag{1}$$

continuity equation

$$\frac{\partial(\rho u)}{\partial x} + \frac{\partial(\rho v)}{\partial y} = 0 \tag{2}$$

energy equation

$$\rho u \frac{\partial T}{\partial x} + \rho v \frac{\partial T}{\partial y} = (\gamma - 1) M_\infty^2 u \frac{dp}{dx} + \frac{1}{RePr} \frac{\partial}{\partial y}\left(\kappa \frac{\partial T}{\partial y}\right) + \frac{(\gamma - 1)}{Re} M_\infty^2 \mu \left(\frac{\partial u}{\partial y}\right)^2 \tag{3}$$

and equation of state for perfect gas

$$\rho T = \rho_e T_e \tag{4}$$

where velocities are normalized with respect to the freestream velocity U_∞^*, lengths are normalized with respect to L*, which is the distance from the leading edge to the center of the imperfection, and the temperature and the viscosity and thermal-conductivity coefficients are normalized with respect to their freestream values T_∞^*, μ_∞^*, and κ_∞^*, respectively. Here,

$$Re = \frac{U_\infty^* L^* \rho_\infty^*}{\mu_\infty^*}, \quad Pr = \frac{\mu_\infty^* C_p^*}{\kappa_\infty^*}, \quad \text{and } \gamma = \frac{C_p^*}{C_v^*} \tag{5}$$

where C_p^* and C_v^* are the gas specific-heat coefficients at constant pressure and volume, respectively.

The boundary conditions at the wall are

$$u = v = 0 \text{ and } T = T_w \quad at \quad y = f[\zeta(x)] \tag{6}$$

where $f(\zeta)$ is the shape of the wall with the imperfections. For the step

$$f(\zeta) = \frac{1}{2} h[1 + \text{erf}(\zeta)], \; \zeta = Re^{-3/8} \lambda^{5/4} (x - 1) \tag{7}$$

and for the hump

$$f(\zeta) = \begin{cases} h(1 - 12\zeta^2 + 16\zeta^3), & \text{if } \zeta \le 0.5 \\ 0.0, & \text{if } \zeta > 0.5 \end{cases}$$

$$\zeta = \left| \frac{(x - 1)}{x_w} \right|$$

where x_w is the width of the hump, erf is the error function, h is the height of the step or the hump, and $\lambda = 0.332057$. Away from the wall

$$u \to U_e \text{ and } T \to T_e \text{ as } y \to \infty \tag{8}$$

where the subscript e stands for edge variables.

Using the Prandtl transposition theorem,

$$z = y - f[\zeta(x)],\ w = v - u\frac{df}{dx} \tag{9}$$

we rewrite Eqs. (1)-(3), (6), and (8) as

$$\rho u\frac{\partial u}{\partial x} + \rho w\frac{\partial u}{\partial z} = -\frac{dp}{dx} + \frac{1}{Re}\frac{\partial}{\partial z}\left(\mu\frac{\partial u}{\partial z}\right) \tag{10}$$

$$\frac{\partial(\rho w)}{\partial x} + \frac{\partial(\rho w)}{\partial z} = 0 \tag{11}$$

$$\rho u\frac{\partial T}{\partial x} + \rho w\frac{\partial T}{\partial z} = (\gamma - 1)M_\infty^2 u\frac{dp}{dx} + \frac{1}{RePr}\frac{\partial}{\partial z}\left(\kappa\frac{\partial T}{\partial z}\right) + \frac{(\gamma - 1)}{Re}M_\infty^2\mu\left(\frac{\partial u}{\partial z}\right)^2 \tag{12}$$

$$u = w = 0,\ T = T_w \text{ at } z = 0 \tag{13}$$

$$U \to U_e \text{ and } T \to T_e \text{ as } z \to \infty \tag{14}$$

Next we use the Levy-Lees variables

$$\xi(x) = \int_0^x \rho_e\mu_e U_e dx \quad \text{and} \quad \eta(x, z) = \frac{\sqrt{Re}\,U_e}{\sqrt{2\xi}}\int_0^z \rho dz \tag{15}$$

and transform Eqs. (10)-(12) into

$$2\xi F F_\xi + VF_\eta - \frac{\partial}{\partial\eta}\left(\theta\frac{\partial F}{\partial\eta}\right) + \beta_0(F^2 - Q) = 0 \tag{16}$$

$$2\xi F_\xi + V_\eta + F = 0 \tag{17}$$

$$2\xi FQ_\xi + VQ_\eta - \frac{\partial}{\partial\eta}\left(\frac{\theta}{Pr}\frac{\partial Q}{\partial\eta}\right) - (\gamma - 1)M_\infty^2\frac{U_e^2}{T_e}\theta F_\eta^2 = 0 \tag{18}$$

where

$$F = \frac{u}{U_e},\quad Q = \frac{T}{T_e} \tag{19a}$$

$$V = \frac{\sqrt{2\xi}}{\rho_e U_e\mu_e}\left[\sqrt{Re}\,\rho w + \eta_x\sqrt{2\xi}\,F\right] \tag{19b}$$

$$\theta = \frac{\rho\mu}{\rho_e\mu_e} \text{ and } \beta_0 = \frac{2\xi}{U_e}\frac{dU_e}{d\xi} \tag{19c}$$

The boundary conditions become

$$F = V = 0 \text{ and } Q = Q_w \text{ at } \eta = 0 \tag{20a}$$

$$F \to 1 \text{ and } Q \to 1 \text{ as } \eta \to \infty \tag{20b}$$

$$F = F(\xi_0, \eta) \text{ and } Q = Q(\xi_0, \eta) \text{ at } \xi = \xi_0 \tag{20c}$$

To account for viscous-inviscid interactions, we need to calculate the inviscid flow over the displaced surface. This is done through the interaction law, which relates the edge velocity to the displacement thickness. Using thin airfoil theory, we obtain

$$U_e = \bar{U}_e + \frac{1}{\beta\pi}\int_{LE}^{\infty} U_e\delta\,\frac{d(\ln\rho_e)/dt}{x-t}\,dt + \frac{1}{\beta\pi}\int_{LE}^{\infty}\frac{d(U_e\delta)/dt}{x-t}\,dt \tag{21}$$

where $\beta = \sqrt{1-M_\infty^2}$, the displacement thickness δ is given by

$$\delta = \frac{1}{\sqrt{Re}}\frac{\sqrt{2\xi}}{\rho_e u_e}\int_0^{\infty}(Q-F)d\eta \tag{22}$$

and $\bar{U}_e$ is the inviscid surface velocity in the absence of the boundary layer, which, in the case of small imperfections, can be expressed as

$$\bar{U}_e = 1 + \frac{1}{\beta\pi}\int_{LE}^{\infty}\frac{df/dt}{x-t}\,dt \tag{23}$$

Defining $\chi = f + U_e\delta$, we rewrite Eq. (21) as

$$U_e = 1 + \frac{1}{\beta\pi}\int_{LE}^{\infty} U_e\delta\,\frac{d(\ln\rho_e)/dt}{x-t}\,dt + \frac{1}{\beta\pi}\int_{LE}^{\infty}\frac{d\chi/dt}{x-t}\,dt \tag{24}$$

The principal values of the integrals in Eq. (24) are assumed.

Following Davis and Werle[20] and Nayfeh et al[8], we integrate the interaction law by parts to eliminate the derivative of χ. We assume χ to vary linearly over a differencing interval to obtain a second-order quadratic expression for the edge velocity. Furthermore, we calculate the second term in Eq. (24) explicitly from the

previous iteration. By assuming the flow far away from the imperfection to be a Blasius flow, we can write the interaction law as

$$V_N + \phi\beta_{oi} = \psi \tag{25}$$

For a definition of ϕ and ψ and a detailed derivation of Eq. (25), we refer the reader to Ref. 6.

Equations (16)-(18) and (20) are solved simultaneously with Eq. (25) using central differences in the vertical direction and three-point backward differencing in the streamwise direction.

Ragab, Nayfeh, and Krishna[21] compared the IBL calculations with solutions of the thin-layer compressible Navier-Stokes equations obtained using the computer code "ARC2D" developed at NASA Ames (Version 1.5 GAMMA). The results obtained using the IBL agree very well with those obtained using the Navier-Stokes solver; this is true for both the mean flow and the stability characteristics. In Ref. 21 insulated wall conditions were used. In the present work, we investigate the influence of continuous and strip cooling.

III. Stability Calculations

In this work, we consider the linear two-dimensional quasi-parallel stability of the mean flow calculated using the interacting boundary-layer formulation. The quasi-parallel assumption was justified a posteriori by Nayfeh et al[6]. They found that the wavelengths of the disturbances are the order of the boundary-layer thickness. The calculations are performed for constant specific heats and Prandtl number. Since we are limiting our calculations to subsonic flows, this assumption has a small effect on the accuracy of the stability results. Moreover, the viscosity and thermal-conductivity coefficients μ and κ are assumed to be functions of temperature only. Since Pr and C_p^* are constant we take $\kappa = \mu$.

To derive the stability equations, we superimpose 2-D disturbances on the mean flow calculated using the interacting boundary-layer formulation to obtain the total flow quantities

$$\overline{\rho} = \rho_m(y) + \rho(x,y,t) \tag{26a}$$

$$\overline{u} = u_m(y) + u(x,y,t) \tag{26b}$$

$$\bar{v} = v(x,y,t) \tag{26c}$$

$$\bar{p} = p_m(y) + p(x,y,t) \tag{26d}$$

$$\bar{\mu} = \mu_m(y) + \mu(x,y,t) \tag{26e}$$

$$\bar{\lambda} = \lambda_m(y) + \lambda(x,y,t) \tag{26f}$$

$$\bar{T} = T_m(y) + T(x,y,t) \tag{26g}$$

where λ and μ appear in the definition of the bulk-viscosity coefficient k as

$$k = \lambda + \frac{2}{3}\mu$$

The subscript m refers to mean-flow quantities and the overbar refers to total flow quantities. Since $\bar{\mu}$ and $\bar{\lambda}$ are functions of temperature only, we have

$$\lambda = \frac{d\lambda_m}{dT_m} T = \lambda'_m(T_m)T \quad \text{and} \quad \mu = \frac{d\mu_m}{dT_m} T = \mu'_m(T_m)T \tag{27}$$

Substituting Eqs. (26) and (27) into the 2-D compressible Navier-Stokes equations, subtracting the mean-flow quantities, and linearizing the resulting equations, we obtain

$$\frac{\partial \rho}{\partial t} + u_m \frac{\partial \rho}{\partial x} + \frac{\partial \rho_m}{\partial y} v + \rho_m \left(\frac{\partial u}{\partial x} + \frac{\partial v}{\partial y} \right) = 0 \tag{28}$$

$$\begin{aligned} \rho_m \left(\frac{\partial u}{\partial t} + u_m \frac{\partial u}{\partial x} + \frac{du_m}{dy} v \right) + \frac{\partial p}{\partial x} \\ - \frac{1}{R} \frac{\partial}{\partial x} \left[r\mu_m \frac{\partial u}{\partial x} + m\mu_m \frac{\partial v}{\partial y} \right] \\ - \frac{1}{R} \frac{\partial}{\partial y} \left[\mu_m \left(\frac{\partial u}{\partial y} + \frac{\partial v}{\partial x} \right) + \mu \frac{du_m}{dy} \right] \end{aligned} \tag{29}$$

$$\begin{aligned} \rho_m \left(\frac{\partial v}{\partial t} + u_m \frac{\partial v}{\partial x} \right) + \frac{\partial p}{\partial y} - \frac{1}{R} \frac{\partial}{\partial y} \left[r\mu_m \frac{\partial v}{\partial y} \right. \\ \left. + m\mu_m \frac{\partial u}{\partial x} \right] - \frac{1}{R} \frac{\partial}{\partial x} \left[\mu_m \left(\frac{\partial v}{\partial x} + \frac{\partial u}{\partial y} \right) + \mu \frac{du_m}{dy} \right] = 0 \end{aligned} \tag{30}$$

$$\rho_m\left(\frac{\partial T}{\partial t}+u_m\frac{\partial T}{\partial x}+\frac{dT_m}{dy}v\right)-(\gamma-1)M_\infty^2\left(\frac{\partial p}{\partial t}+u_m\frac{\partial p}{\partial x}\right)$$
$$=\frac{\mu_m}{RPr}\left(\frac{\partial^2 T}{\partial x^2}+\frac{\partial^2 T}{\partial y^2}\right)+\frac{1}{RPr}\frac{\partial\mu}{\partial y}\frac{dT_m}{dy} \tag{31}$$
$$+\frac{1}{RPr}\frac{d\mu_m}{dy}\frac{dT}{dy}+\frac{(\gamma-1)M_\infty^2\phi}{R}+\frac{\mu}{RPr}\frac{d^2T_m}{dy^2}$$

where

$$\phi=2\mu_m\left[\left(\frac{\partial u}{\partial y}+\frac{\partial v}{\partial x}\right)\frac{du_m}{dy}\right]+\mu\left(\frac{du_m}{dy}\right)^2 \tag{32}$$

$$m=\frac{\lambda_m}{\mu_m},\ r=2+m, \tag{33}$$

$$R=\frac{U_\infty^*\delta_0^*}{\nu_\infty^*},\quad \delta_0^*=\sqrt{\frac{\nu_\infty^* x^*}{U_\infty^*}} \tag{34}$$

The linearized equation of state for a perfect gas is

$$\gamma M_\infty^2 p=\rho_m T+\rho T_m$$

or

$$\rho=(\gamma M_\infty^2 p-\rho_m T)/T_m \tag{35}$$

The boundary conditions are

$$u=v=0,\ T=0\quad\text{at}\quad y=0 \tag{36}$$

$$u,v,p,T\to 0\quad\text{as}\quad y\to\infty \tag{37}$$

Since the coefficients in Eqs. (28)-(31), (36), and (37) are functions of y only, we seek normal-mode solutions of the form

$$q=\hat{q}(y)\exp\{i\int\alpha dx-i\omega t\}+\text{complex conjugate} \tag{38}$$

where q stands for (u, v, p, T), α is the wave number, and ω is the frequency. For spatial stability analysis α is complex and ω is real, whereas for temporal-stability analysis ω is complex and α is real. In this work, we analyze the spatial stability case and determine ω from the nondimensional frequency F as $\omega=F/R$.

Dropping the hat from $\hat{q}$ for convenience and defining

$$\Omega = \omega - \alpha u_m \tag{40}$$

we find that α is governed by the eigenvalue problem

$$Dv = -i\alpha u + \frac{DT_m}{T_m} v + \frac{i\Omega p}{p_m} - \frac{i\Omega T}{T_m} \tag{41}$$

$$\begin{aligned} D^2u = &\left(\frac{-i\rho_m \Omega R}{\mu_m} + r\alpha^2 \right) u - \left(\frac{\mu'_m DT_m}{\mu_m} Du \right) \\ &+ \left[\frac{\rho_m R Du_m}{\mu_m} - i\alpha \frac{\mu'_m DT_m}{\mu_m} \right] v - i(1+m)\alpha Dv \\ &+ \frac{iR\alpha}{\mu_m} p - \left[\frac{Du_m}{\mu_m} D(\mu'_m) \frac{D^2u_m}{\mu_m} \mu'_m \right] T - \frac{\mu'_m}{\mu_m} Du_m DT \end{aligned} \tag{42}$$

$$\begin{aligned} \chi_0 Dp = &-i\alpha \left(r \frac{DT_m}{T_m} + \frac{2\mu'_m DT_m}{\mu_m} \right) u - i\alpha Du + \left(\frac{iR\Omega}{\mu_m T_m} - \alpha^2 + r \frac{D^2T_m}{T_m} + \frac{r\mu'_m (DT_m)^2}{\mu_m T_m} \right) v \\ &+ i \frac{r}{p_m} \left[\Omega \left(\frac{DT_m}{T_m} + \frac{\mu'_m}{\mu_m} DT_m \right) - \alpha Du_m \right] p \\ &+ \left[i(\alpha Du_m) \left(\frac{\mu'_m}{\mu_m} + \frac{r}{T_m} \right) - \frac{ir\Omega\mu_m}{\mu_m} DT_m \right] T - \frac{ir\Omega}{T_m} DT \end{aligned} \tag{43}$$

$$\begin{aligned} D^2T = &-2(\gamma-1)M_\infty^2 Pr Du_m Du + \left[RPr \frac{\rho_m DT_m}{\mu_m} - 2i(\gamma-1)M_\infty^2 Pr\alpha Du_m \right] v \\ &+ i(\gamma-1)M_\infty^2 PrR \frac{\Omega}{\mu_m} p + \left[-iRPr\Omega \frac{\rho_m}{\mu_m} + \alpha^2 - \frac{(DT_m)^2 d\mu_{m'}}{\mu_m dT_m} \right. \\ &\left. - \mu'_m \frac{D^2T_m}{\mu_m} - (\gamma-1)\ M_\infty^2 Pr \frac{\mu'_m}{\mu_m} (Du_m)^2 \right] T - 2 \frac{\mu'_m DT_m}{\mu_m} DT \end{aligned} \tag{44}$$

$$u = v = T = 0 \quad \text{at} \quad y = 0 \tag{45}$$

$$u, v, p, T, \to 0 \quad \text{as} \quad y \to \infty \tag{46}$$

where

$$D = \frac{d}{dy}\ ,\ \chi_0 = \frac{R}{\mu_m} - ir \frac{\Omega}{p_m}\ ,\ \text{and}\ p_m = \frac{1}{\gamma M_\infty^2} \tag{47}$$

IV. Numerical Results

Following the procedure described in section II, we calculated the mean flow over a backward-facing step for different wall temperatures. Figure 1 shows the influence of cooling on the skin-friction coefficient

$$C_f = \frac{2U_e^2\mu(T_w)}{T_w\sqrt{2Re\xi}}\frac{\partial F}{\partial \eta}\Big|_{\eta=0} \tag{48}$$

In the case of cooling, the separation point is almost fixed but the reattachment point moves slightly upstream, resulting in a slightly smaller separation bubble. Moreover, cooling causes a larger negative shear prior to reattachment. The pressure coefficient $C_p = 2(\rho_e T_e - 1)/(\gamma M_\infty^2)$ is plotted in Fig. 2. Although cooling does not have much effect on C_p far away from the imperfection, it causes steeper adverse and favorable pressure gradients around the separation bubble. In Fig. 3, we compare the mean profiles of the flows over adiabatic and cooled walls at several locations. In general, cooling results in fuller velocity profiles compared to the adiabatic case. In the separation region, although the mean-velocity profiles are still fuller away from the wall for the cooled wall case, they develop inflection points close to the wall, and more negative flows develop near reattachment. The corresponding temperature profiles are shown in Fig. 4. The combined effect of cooling on the velocity and temperature profiles is a movement of the generalized inflection point closer to the wall in the separation region, as shown in Fig. 5.

For a given mean flow, ω, and R, we solved for the eigenvalue α and the eigenfunctions, and then determined the amplification factor from

$$N = -\int_{R_0}^{R} 2\alpha_i dR \tag{49}$$

where R_0 corresponds to Branch I of the neutral stability curve and α_i is the imaginary part of α . The eigenvalue problem was solved using the second-order finite-difference subroutine DBVPFD[22], which is much faster than SUPORT[23]; the results of DBVPFD are in full agreement with those of SUPORT. In all the cases, the results are for the most dangerous frequency, defined to be the one that results in an N factor of 9.0 in the shortest distance[6,21]. In the case of cooling it is the one resulting in the largest N factor in the shortest distance. It turns out that the most dangerous frequency for cooled and adiabatic wall are about the same. Figure 6

shows the N factor for various frequencies when $T_w = 0.55T_{ad}$. It appears that $F = 50x10^{-6}$ produces the largest N factor.

We analyzed the stability of the mean profiles calculated using the IBL code for flows over a backward-facing step. The present analysis accounts for both viscous and shear-layer instabilities in the separation region. The effect of wall cooling on the stability of such flows is different from that on the stability of flows over flat plates. Figure 7 shows the growth rates for the cases of adiabatic and cooled walls. The temperature of the cooled wall is 55% of the adiabatic wall temperature T_{ad}. We note that the instability is due to the viscous mechanism in the attached region and due to a combination of the viscous and shear-layer mechanisms in the separation region. Figure 7 shows that cooling decreases the growth rates and hence it is stabilizing in the attached flow regions because cooling produces fuller velocity profiles. On the other hand, in the separation region cooling increases the growth rates due to the increase in the negative shear flow in the separation bubble and the movement of the generalized inflection points closer to the cooled wall. However, the growth-rate curve corresponding to the cooled case is narrower around the peak value than that corresponding to the adiabatic case because the cooled flow reattaches ahead of the adiabatic flow. Figure 8 shows the variation of the growth rate with streamwise distance for different wall temperatures. Decreasing the wall temperature destabilizes the flow in the separation bubble and stabilizes it in the attached flow region. Moreover the growth-rate curve gets narrower as the wall temperature decreases. Consequently, the overall effect of cooling as measured by the N factor depends on the wall temperature, as shown in Fig. 9. When $T_w = 0.95T_{ad}$, the boundary layer is completely stable ahead of separation and the overall N factor is less than that of the adiabatic wall. As T_w decreases below 0.8 T_{ad} the increase in the growth rates in the separation region overcomes the reduction in the growth rates elsewhere, and the net result is an increase in the maximum N factor.

For a Mach number of 0.8, Fig. 10 shows the growth rates for various wall temperatures. The increase in the growth rates in the separation region when M_∞ = 0.8 is less than that when M_∞ = 0.5. Moreover, the peak growth rate when M_∞ = 0.8 is wider than that when M_∞ = 0.5. This makes the optimum wall temperature to be at $T_w = 0.6T_{ad}$ as it is clear from the resulting N factors shown in Fig. 11. Figure 11 also shows that at $M_\infty = 0.8$ cooling has a slightly smaller effect than at $M_\infty = 0.5$.

The previous results seem to be general and apply to other imperfections. For example, Figure 12 shows the growth rates for a flow at $M_\infty = 0.8$ around a cubic

hump. The hump width is 0.2 L^* and height is 0.003 L^*. The behavior of the growth rates with cooling is similar to that of the step case. The resulting N factors are plotted in Fig. 13. This figure shows that the optimum wall temperature is about $T_w = 0.8T_{ad}$. When $T_w = 0.6T_{ad}$ the N factor is about the same as that for the adiabatic wall.

In an attempt to lower the growth rates in the separation region, we performed calculations for a wall that is cooled everywhere except in the separation bubble. The results indicate that this distribution has a very small effect on the N factor as shown in Fig. 14. The growth rates are slightly changed as shown in Fig. 15. The reason for this small effect is that the mean profiles in the separated region are influenced by the cooling ahead of the separation bubble due to the nonsimilarity of the boundary layer.

Next we show the influence of the step position on the N factors for a constant frequency. The results shown in Fig. 16 are for $M_\infty = 0.5$ and adiabatic wall conditions. Unlike the incompressible case the most dangerous step location is not the one corresponding to Branch I of the neutral stability curve, but it is the one corresponding to a distance half-way between Branches I and II. Figure 17 shows that a similar trend is true for the cubic hump.

From the previous results it is clear that the coexistence of viscous- and shear-layer instability mechanisms complicates the effect of cooling on the stability of such flows. Since cooling decreases the viscous instability and increases the shear-layer instability, there exist an optimum wall temperature that considerably reduces the amplification factor.

Acknowledgement

This work was supported by the National Aeronautics and Space Administration under Grant No. NAG-1-714 and the Office of Naval Research under Grant No. N00014-85-K-0011, NR 4325201.

References

1. B. J. Holmes, C. J. Obara, G. L. Martin, and C. S. Domack, *NASA CP 2413,* 1986.

2. B. J. Holmes, C. J. Obara, and L. P. Yip, *NASA TP 2256,* 1984.

3. C. J. Obara and B. J. Holmes, *NASA TP 2414,* 1985.

4. A. Fage, *British Aeronautical Research Council* 2120, 1943.

5. P. S. Klebanoff and K. R. Tidstrom, *Phys. Fluids* 15, 1173 (1972).

6. A. H. Nayfeh, S. A. Ragab, and A. A. Al-Maaitah, *Phys. Fluids* 31, 796 (1988).

7. W. S. Walker and J. R. Greening, *British Aeronautical Research Council* 5950, 1942.

8. H. Bestek, K. Gruber, and H. Fasel, presented at *The Fourth Asian Congress of Fluid Mechanics,* Hong Kong, August 19-23, 1988.

9. S. Burnel, P. Gougat, and F. Martin, *NASA TM-76558,* 1981.

10. P. Gougat and F. Martin, *NASA TM-76559,* 1981.

11. P. Vijgen, S. Doddple, B. Holmes, and C. Van Dam, *J. Aircraft* 25, 776 (1988).

12. E. Hastings, J. Schoenster, C. Obara, and S. Dodbele, *AIAA Paper No. 86-1629,* 1986.

13. W. Asrar and A. H. Nayfeh, *Phys. Fluids* 28, 1263 (1985).

14. A. R. Wazzan, T. T. Okamura, and A. M. O. Smith, *Trans. ASME Ser. C* 90, 109 (1968).

15. A. R. Wazzan, T. T. Okamura, and A. M. O. Smith, in *Proceedings of the 4th International Heat Transfer Conference,* edited by U. Grigul and E. Hahne (Elsevier, Amsterdam, 1970), Vol. 2, Paper No. FC1.4.

16. M. C. Potter and E. Garber, *Phys. Fluids* 15, 387 (1972).

17. L. M. Mack, *Jet Propulsion Lab,* Document 900-277 (Rev. A), Pasadena, CA (1969).

18. M. R. Malik, *AIAA Paper No. 87-1414,* 1987.

19. R. T. Davis, *AIAA Paper No. 84-1614,* 1984.

20. R. T. Davis and M. J. Werle, in *Numerical and Physical Aspects of Aerodynamics Flows,* edited by T. Cebeci (Springer, Berlin, 1982), p. 187.

21. S. A. Ragab, A. H. Nayfeh, and R. C. Krishna, submitted for publication, *Phys. Fluids* .

22. V. Pereyra, in *Lecture Notes in Computer Science,* 76, edited by B Childs, M. Scott, J. W. Daniel, E. Denman, and P. Nelson, (Springer, Berlin 1976), p. 67.

23. R. R. Scott and H. A. Watts, *SIAM J. Num. Anal.* 14, 40 (1977).

Figure Captions

Figure 1. Effect of wall cooling on the shear coefficient for a flow over a backward-facing step when the step height = 0.003, step slope = - 4.34695, M_∞ = 0.5, Re = 1.0x10^6, and Pr = 0.72: ___ T_w/T_{ad} = 1.0, —·— T_w/T_{ad} = 0.8, and - - - T_w/T_{ad} = 0.55 .

Figure 2. Effect of wall cooling on the pressure coefficients for a flow over a backward-facing step when the step height = 0.003, step slope = -4.34695, M_∞ = 0.5, Re = 1.0x10^6, and Pr = 0.72: ___ T_w/T_{ad} = 1.0, —·— T_w/T_{ad} = 0.8, and - - - T_w/T_{ad} = 0.55 .

Figure 3. Effect of wall cooling on the streamwise velocity profiles along the plate when the step height = 0.003, step slope = -4.34965, M_∞ = 0.5, Re = 1.0x10^6, and Pr = 0.72. The profiles correspond to the following values of R starting from left to right: 985, 992, 997, 1012, 1027, 1037, 1042, and 1051. The separation bubble for the cooled wall starts at R = 997 and ends at R = 1037: ___ T_w/T_{ad} = 1.0, and - - - T_w/T_{ad} = 0.55.

Figure 4. Effect of wall cooling on the temperature profiles along the plate when the step height = 0.003, step slope = -4.34965, M_∞ = 0.5, Re = 1.0x10^6, and Pr = 0.72. The profiles correspond to the following values of R starting from left to right: 985, 992, 997, 1012, 1027, 1037, 1042, and 1051. The separation bubble for the cooled wall starts at R = 997 and ends at R = 1037: ___ T_w/T_{ad} = 1.0, and - - - T_w/T_{ad} = 0.55.

Figure 5. Variation of the inflection point across the separation region for adiabatic and cooled-wall conditions when the step height = 0.003, step slope = – 4.34695 , M_∞ = 0.5, Re = 1.0x10^6, and Pr = 0.72: ——— • T_w/T_{ad} = 0.8, and- – – T_w/T_{ad} = 1.0.

Figure 6. The influence of the frequency on the N factor when $T_w = 0.55\,T_{ad}$, step height = 0.003, step slope = - 4.34965, $M_\infty = 0.5$, $Re = 10x10^{-6}$, and Pr = 0.72: ___ $F = 40x10^{-6}$, - - - $F = 60x10^{-6}$, and —·· $F = 50x10^{-6}$.

Figure 7. The growth rates for the flow over cooled and adiabatic walls when the step height = 0.003, step slope = - 4.34965, $M_\infty = 0.5$, $Re = 10x10^6$, Pr = 0.72, and $F = 50x10^{-6}$: ___ $T_w/T_{ad} = 1.0$ and —·· $T_w/T_{ad} = 0.55$.

Figure 8. Variation of the growth rates with wall temperature: step height = 0.003, step slope = - 4.34695, M_∞ = 0.5, Re = $1.0x10^6$, Pr = 0.72, and F = $50x10^{-6}$.

Figure 9. Variation of the amplification factor with wall temperature: step height = 0.003, step slope = - 4.34695, M_∞ = 0.5, Re = $1.0x10^6$, Pr = 0.72, and F = $50x10^{-6}$.

Figure 10. Variation of the growth rates with wall temperature: step height = 0.003, step slope = - 4.34695, M_∞ = 0.8, Re = $1.0x10^6$, Pr = 0.72, and F = $50x10^{-6}$.

Figure 11. Variation of the amplification factor with wall temperature: step height = 0.003, step slope = - 4.34695, M_∞ = 0.8, Re = $1.0x10^6$, Pr = 0.72, and F = $50x10^{-6}$.

Figure 12. Variation of the growth rates with wall temperature for a cubic hump: hump height = 0.003, $x_w = 0.2$, $M_\infty = 0.8$, $Re = 1.0x10^6$, $Pr = 0.72$, and $F = 50x10^{-6}$.

Figure 13. Variation of the amplification factor with wall temperature for a cubic hump: hump height = 0.003, x_w = 0.2, M_∞ = 0.8, Re = $1.0x10^6$, Pr = 0.72, and F = $50x10^{-6}$.

Figure 14. Effect of an adiabatic separation region on the amplification factor: step height = 0.003, step slope = - 4.34695, M_∞ = 0.5, Re = 1.0x10^6, Pr = 0.72, and F = 50x10^{-6}: ___ adiabatic wall, —·· T_w/T_{ad} = 0.8, - - - cooled everywhere except in separation region.

Figure 15. Effect of an adiabatic separation region on the growth rates: step height = 0.003, step slope = - 4.34695, M_∞ = 0.5, Re = 1.0x10^6, Pr = 0.72, and F = 50x10^{-6} : ___ adiabatic wall, —·· T_w/T_{ad} = 0.8, - - - cooled everywhere except in separation region.

Figure 16. Effect of step location on the amplification factor: step height = 0.003; step slope = - 4.34695, M_∞ = 0.5, Re = 1.0x10^6, Pr = 0.72, and F = 50x10^{-6}.

Figure 17. Effect of hump location on the amplification factor: hump height = 0.003, hump width = 0.2, M_∞ = 0.5, Re = 1.0x10^6, Pr = 0.72, and $F = 50x10^{-6}$.

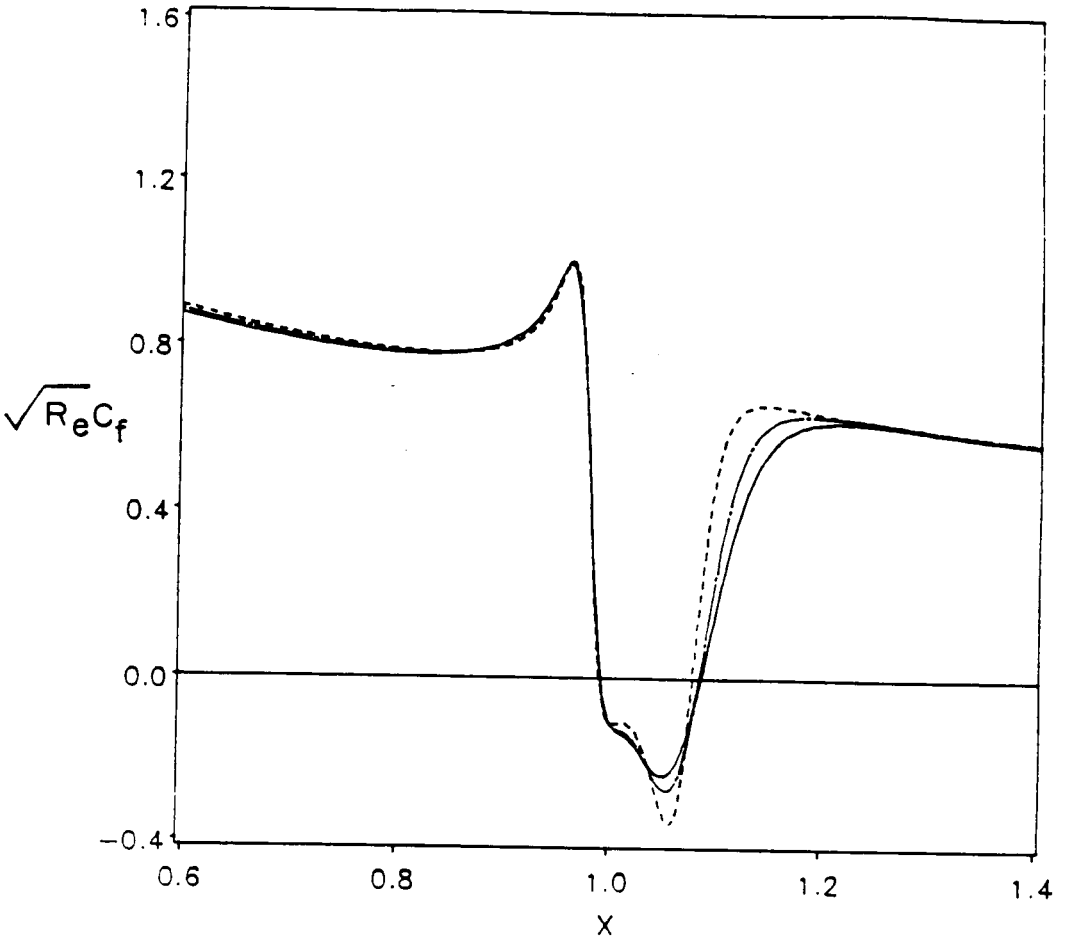
1.6
1.2
0.8
0.4
0.0
−0.4
$\sqrt{R_e}C_f$
0.6
0.8
1.0
1.2
1.4
X

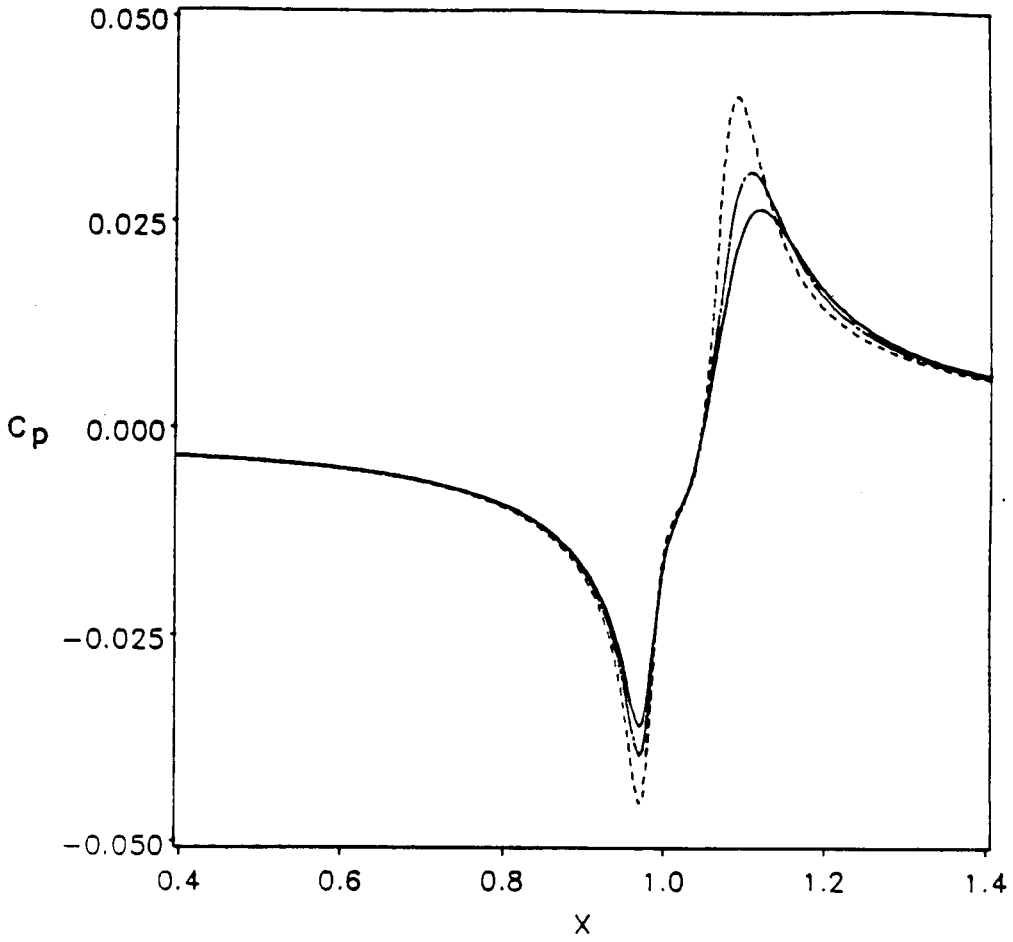
0.050
0.025
0.000
−0.025
−0.050
C_p
0.4
0.6
0.8
1.0
1.2
1.4
X

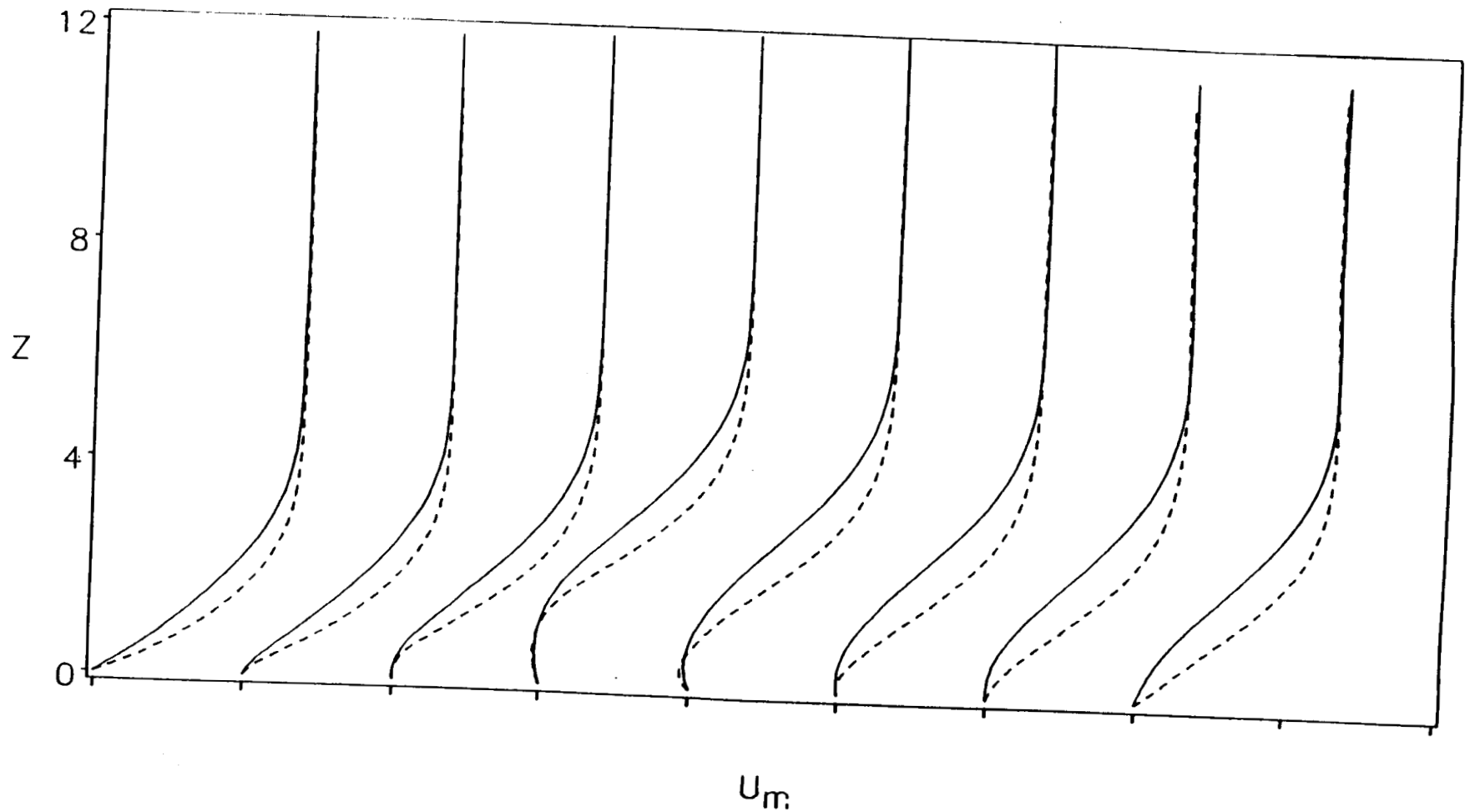
12
8
4
0
Z
U_m

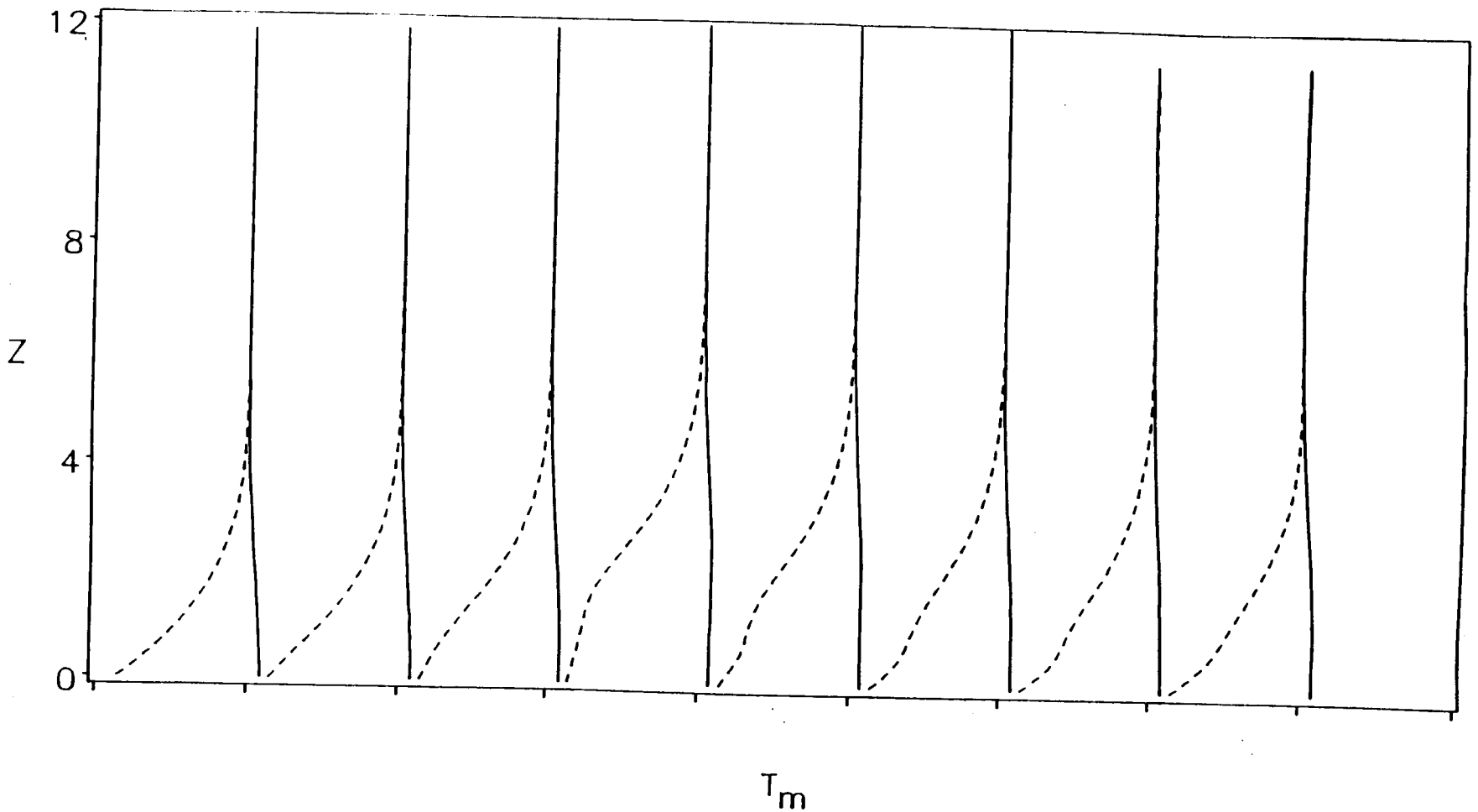
12
8
4
0
Z
T_m

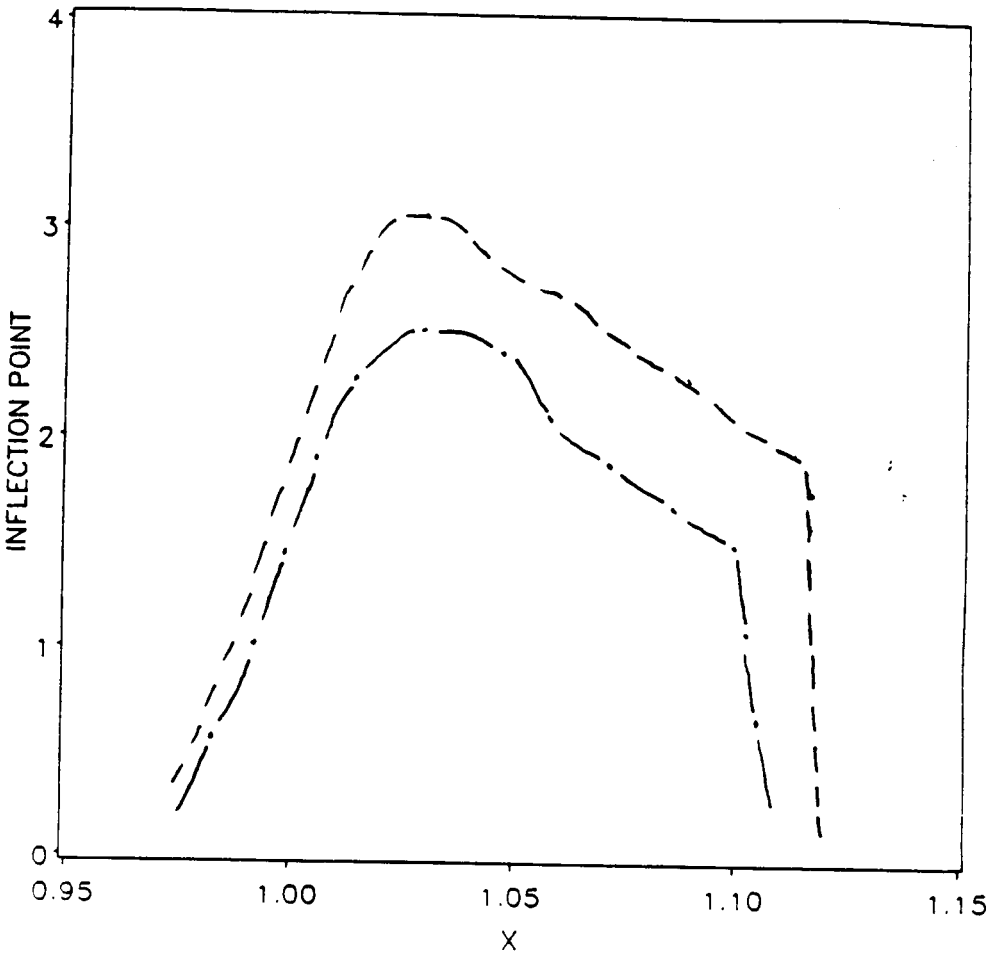
INFLECTION POINT
4
3
2
1
0
0.95
1.00
1.05
1.10
1.15
X

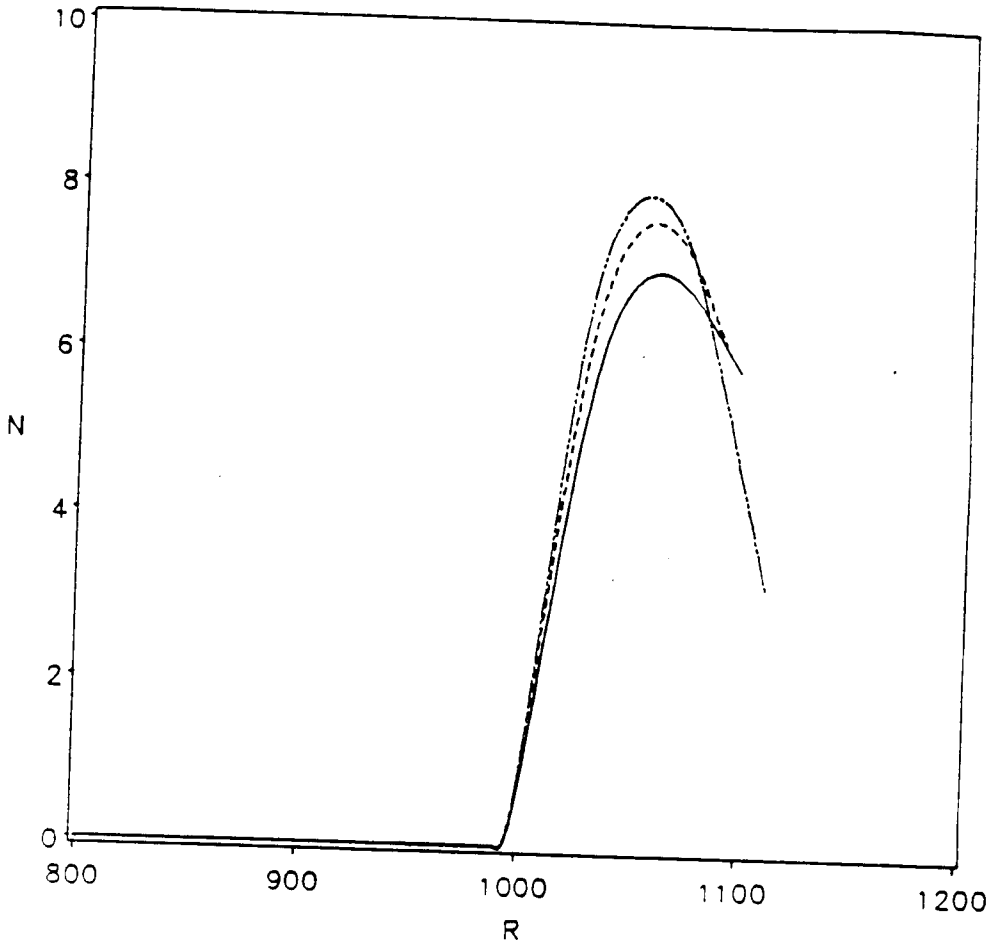
10
8
6
N
4
2
0
800
900
1000
1100
1200
R

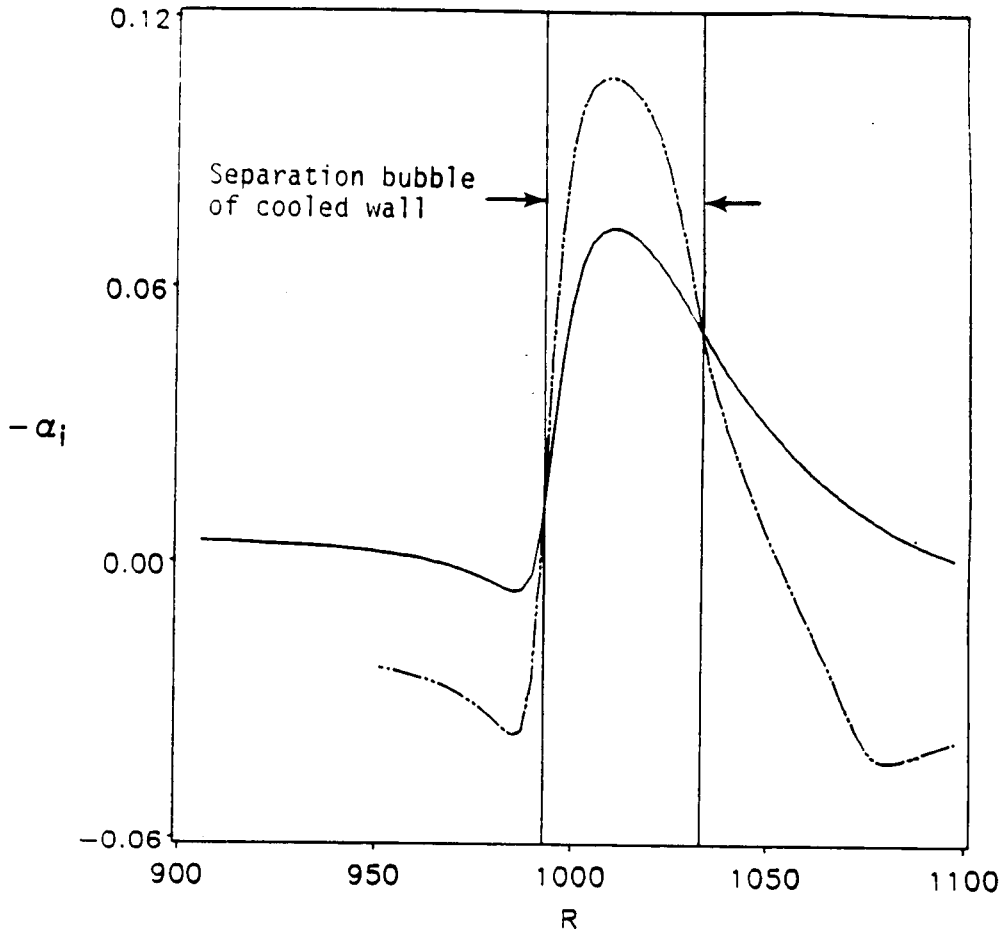
0.12
0.06
0.00
−0.06
$-\alpha_i$
Separation bubble
of cooled wall
900
950
1000
1050
1100
R

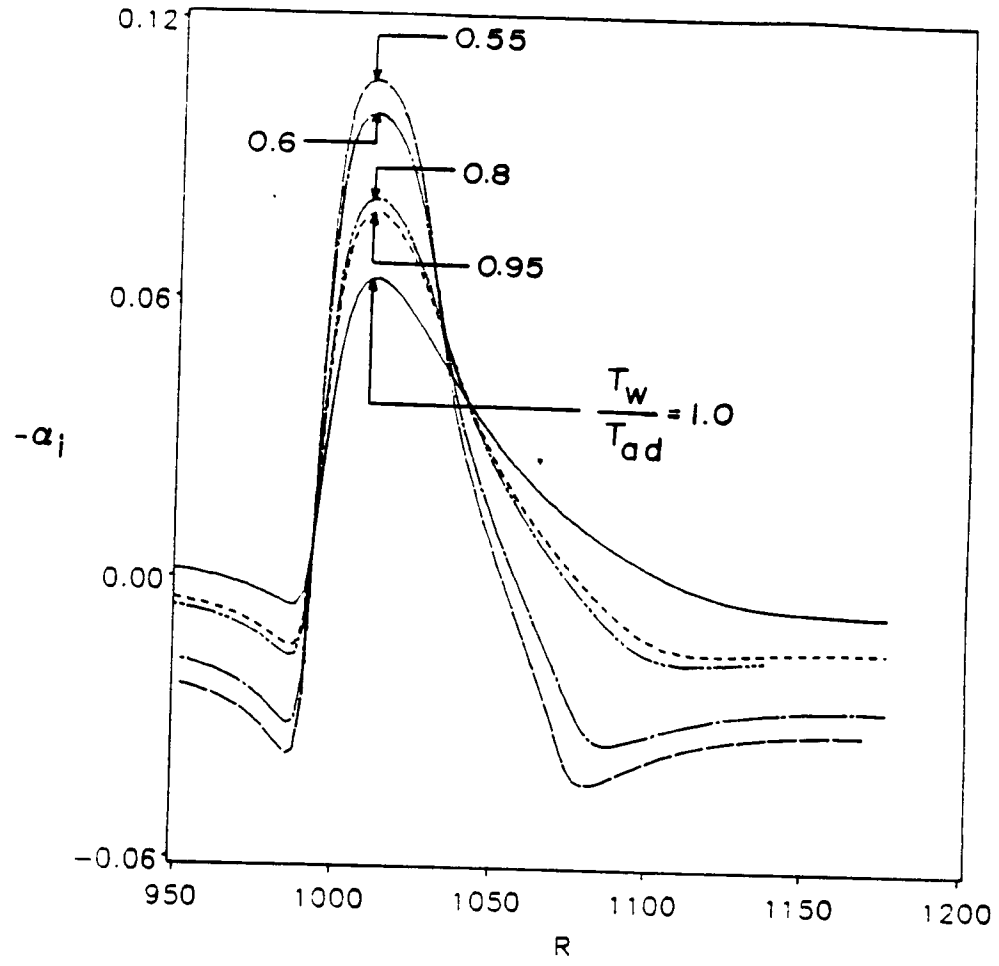
0.12
0.06
0.00
−0.06
$-\alpha_i$
0.55
0.6
0.8
0.95
$\frac{T_w}{T_{ad}} = 1.0$
950
1000
1050
1100
1150
1200
R

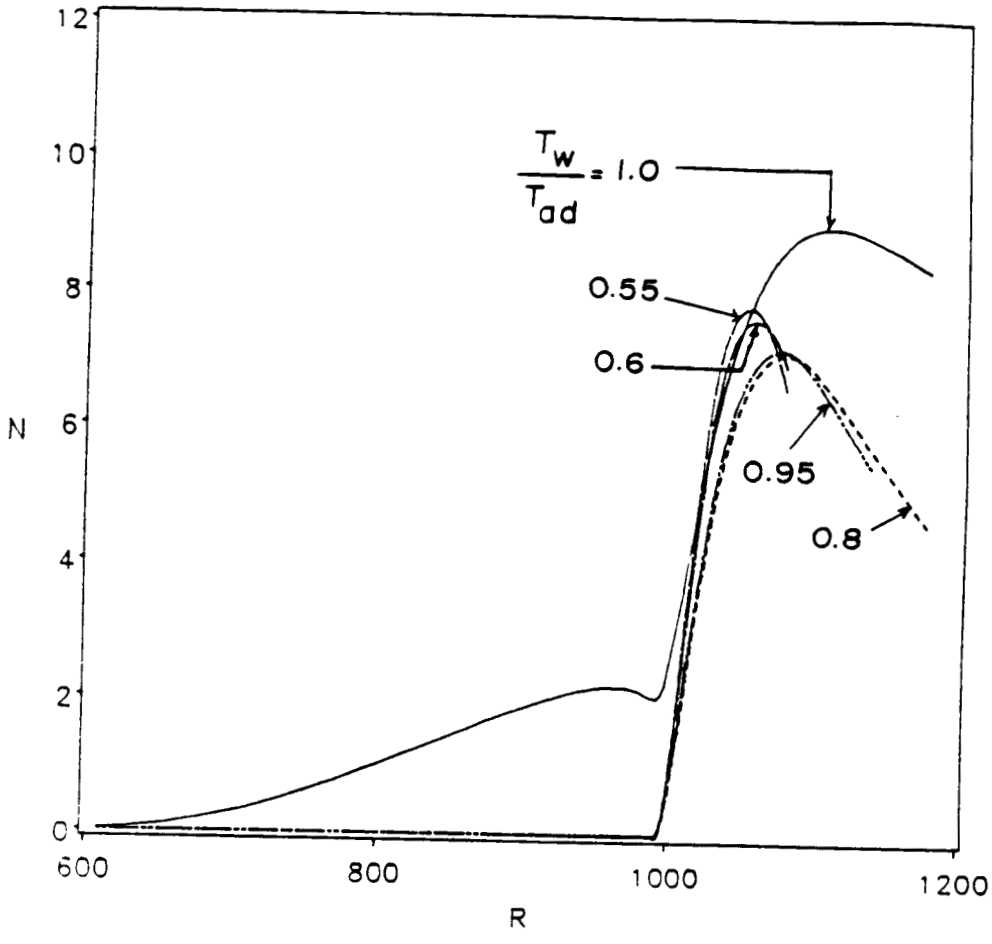
12
10
8
6
4
2
0
N
600
800
1000
1200
R
$\frac{T_w}{T_{ad}} = 1.0$
0.55
0.6
0.95
0.8

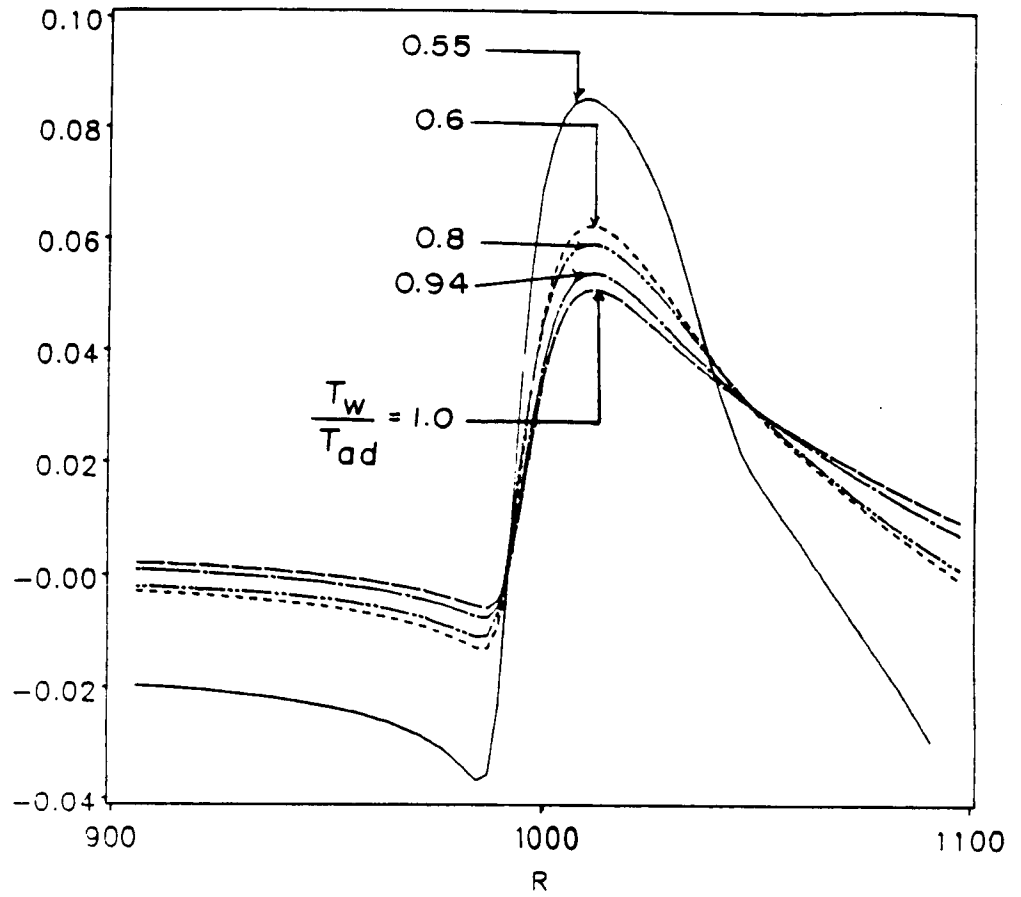
0.10
0.08
0.06
0.04
0.02
−0.00
−0.02
−0.04
900
1000
1100
R
0.55
0.6
0.8
0.94
$\frac{T_w}{T_{ad}} = 1.0$
$-\alpha_i$

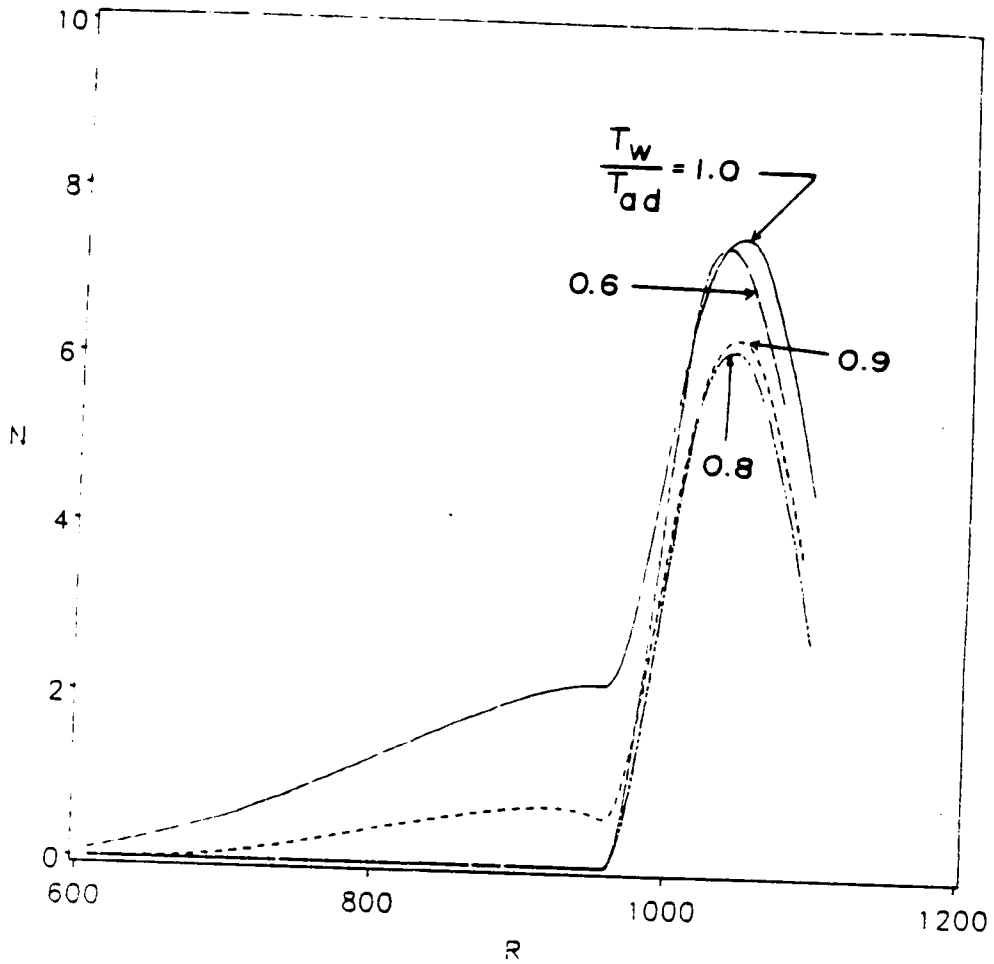
10
8
6
4
2
0
N
600
800
1000
1200
R
$\frac{T_w}{T_{ad}} = 1.0$
0.6
0.9
0.8

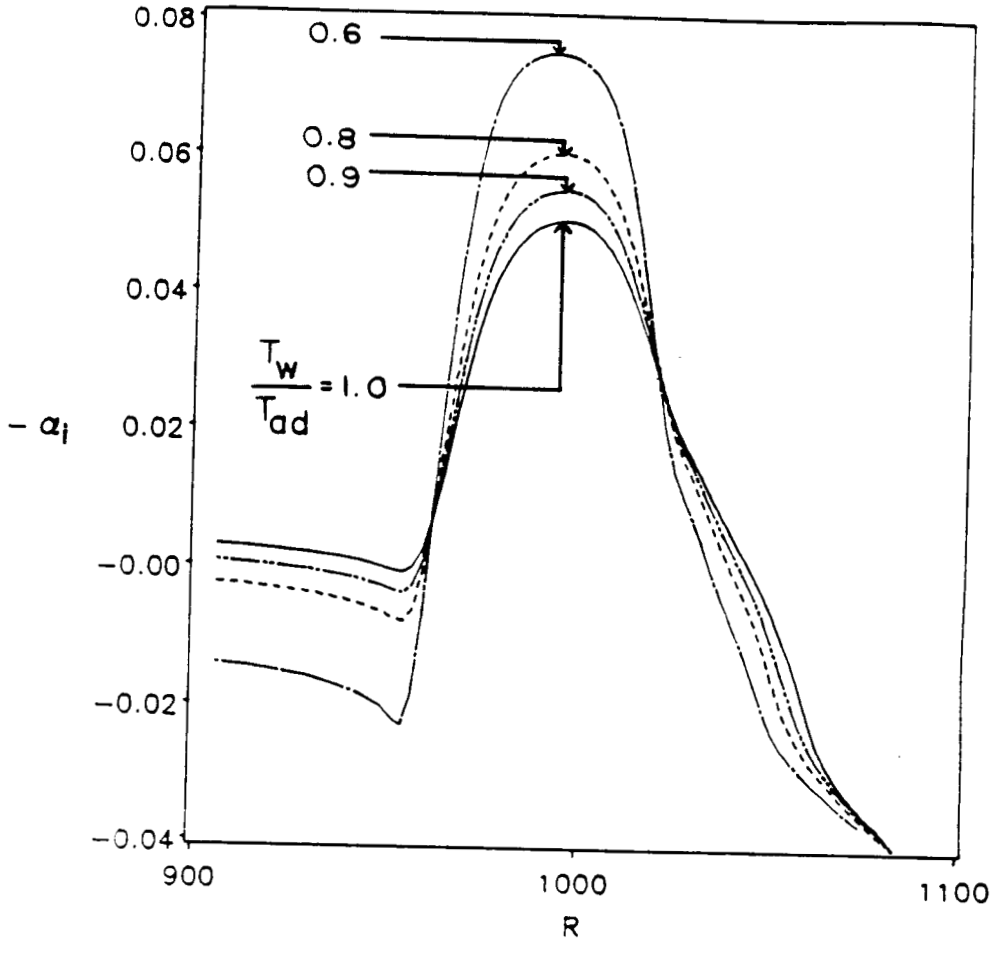
0.08
0.06
0.04
0.02
−0.00
−0.02
−0.04
$-\alpha_i$
0.6
0.8
0.9
$\frac{T_w}{T_{ad}} = 1.0$
900
1000
1100
R

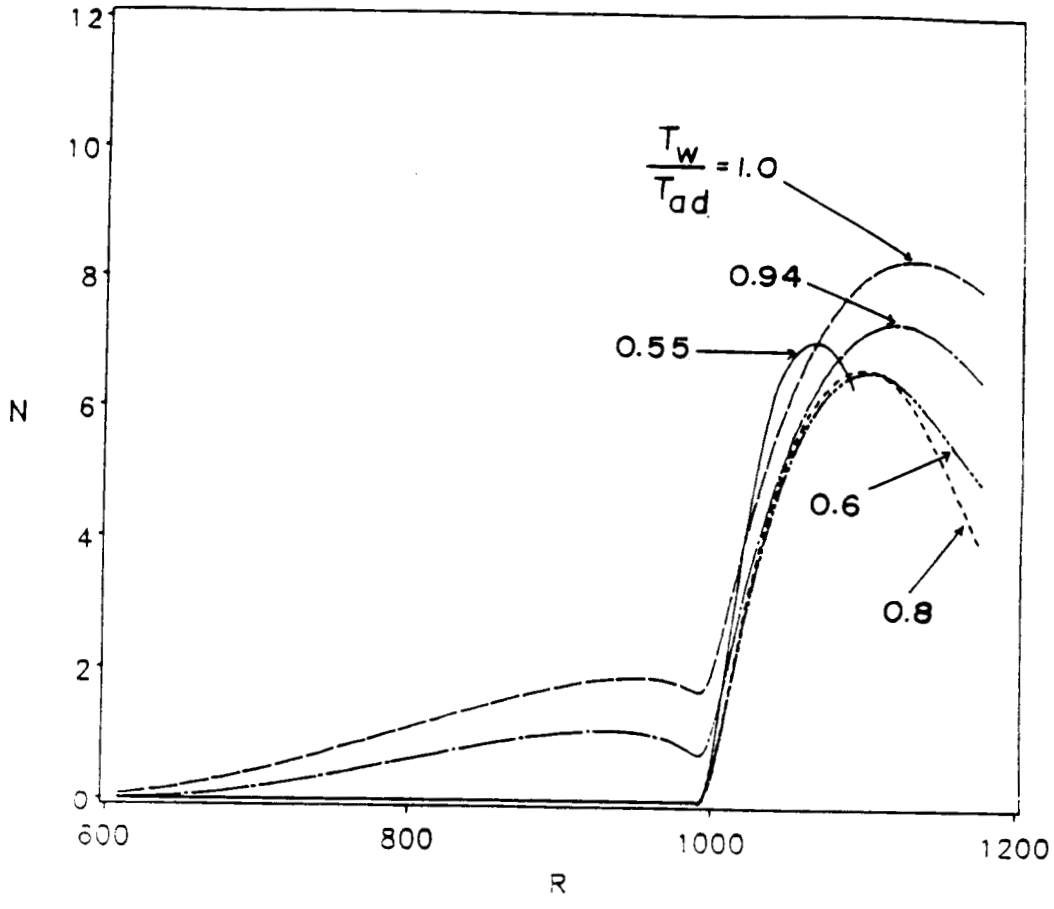
12
10
8
6
4
2
0
N
600
800
1000
1200
R
$\frac{T_w}{T_{ad}} = 1.0$
0.94
0.55
0.6
0.8

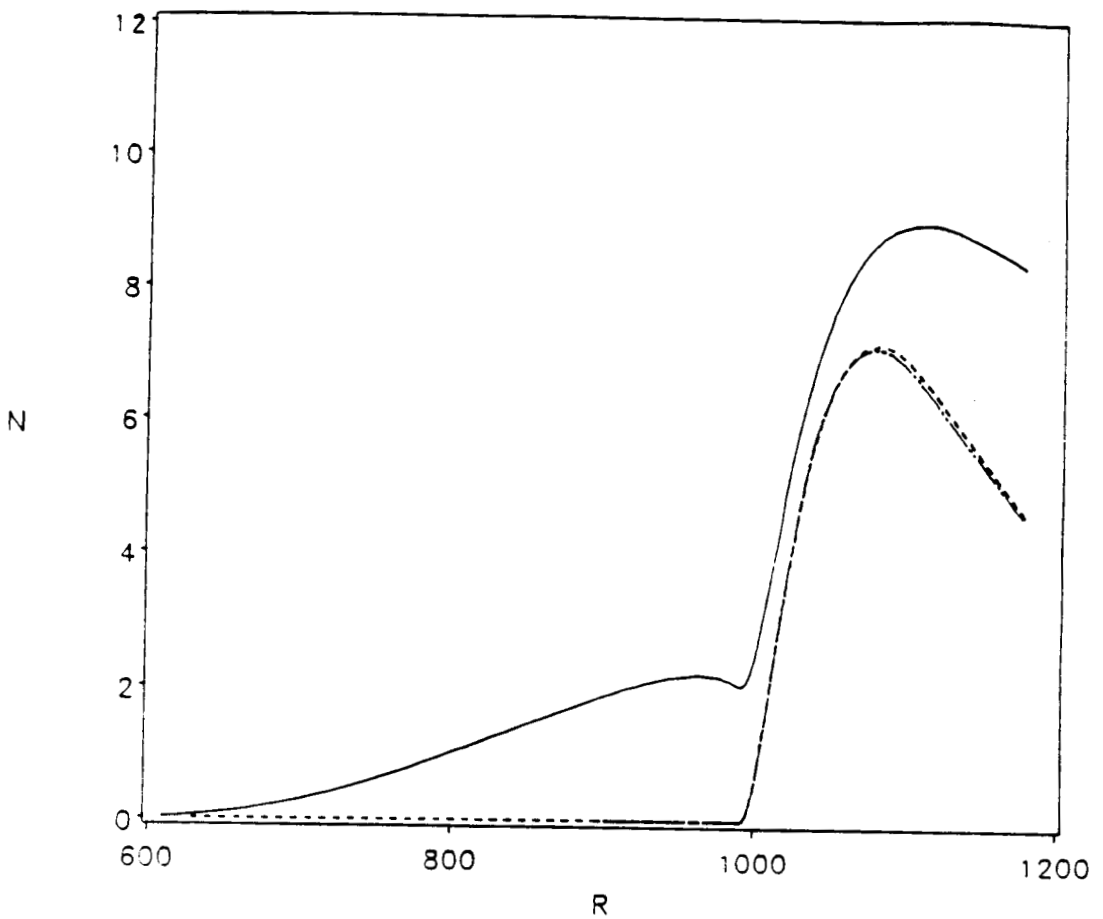
12
10
8
6
4
2
0
N
600
800
1000
1200
R

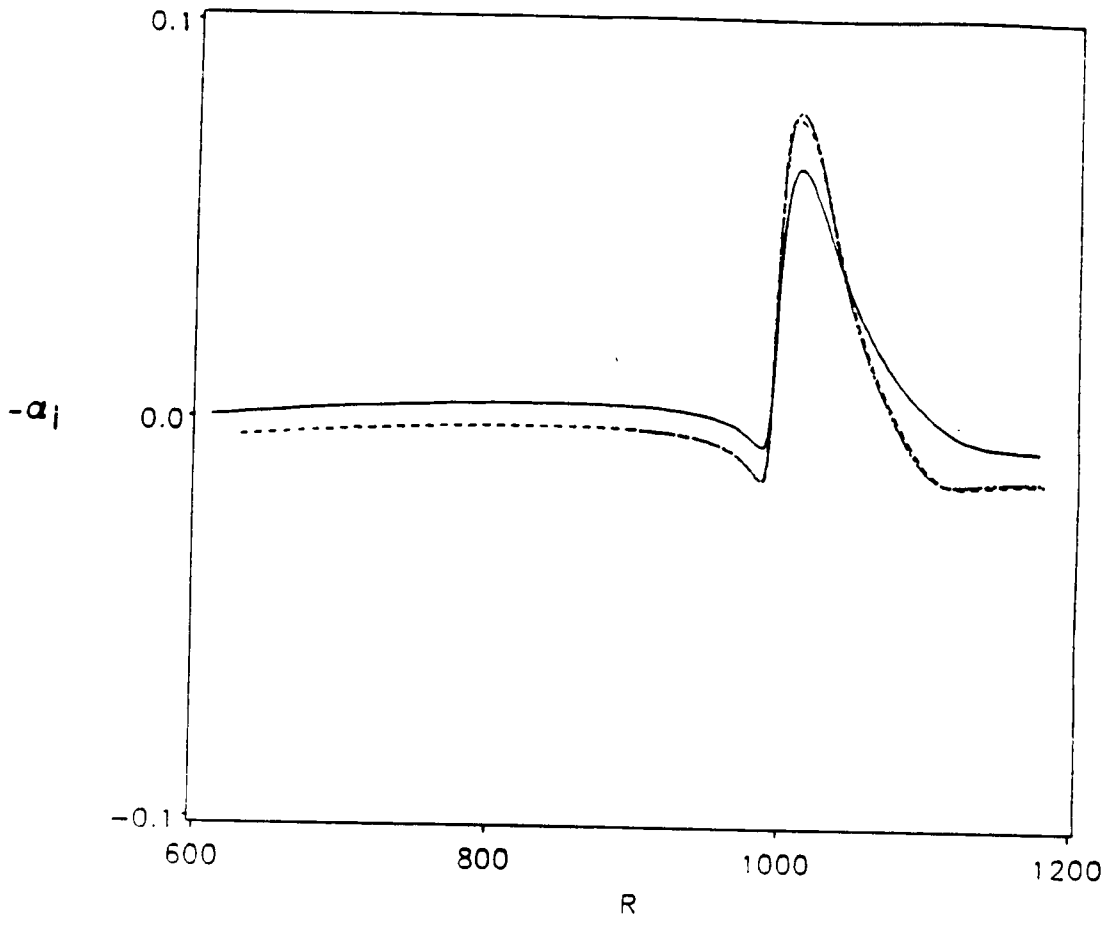
0.1
0.0
-0.1
$-\alpha_i$
600
800
1000
1200
R

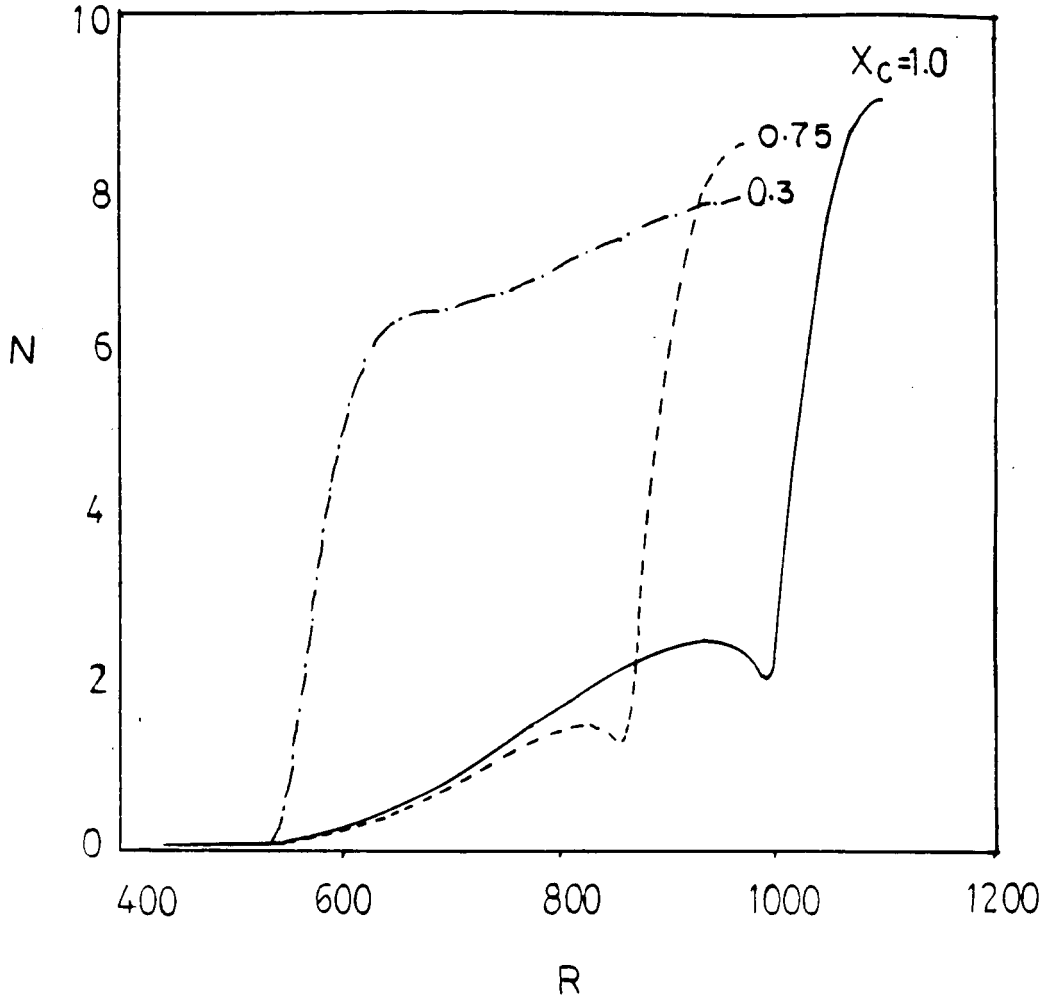
10
8
6
4
2
0
N
400
600
800
1000
1200
R
X_C=1.0
0.75
0.3

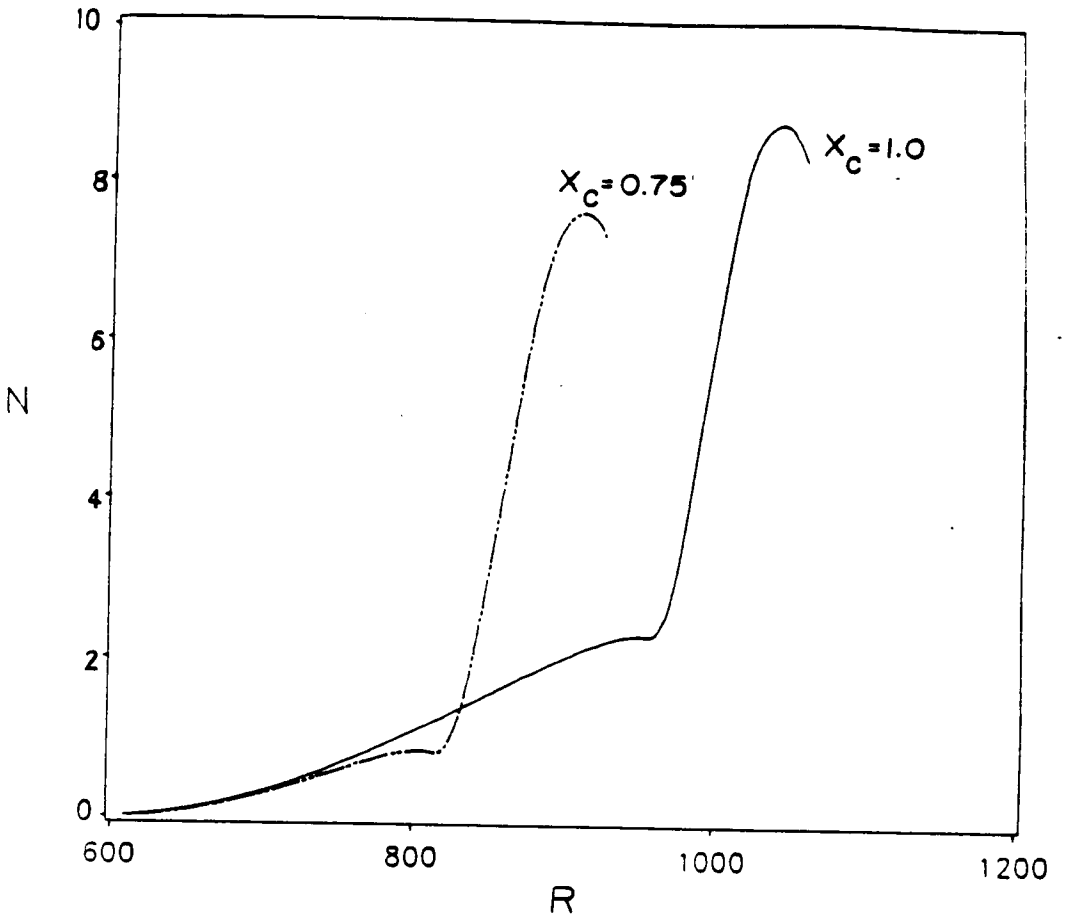
10
8
6
4
2
0
N
600
800
1000
1200
R
X_c=0.75
X_c=1.0